Restricting the Ligand-Linked Heme Movement in *Scapharca* Dimeric Hemoglobin Reveals Tight Coupling between Distal and Proximal Contributions to Cooperativity†

James E. Knapp,‡ Quentin H. Gibson,§ Lauren Cushing,‡ and William E. Royer, Jr.*,‡

Department of Biochemistry and Molecular Pharmacology, University of Massachusetts Medical School, Worcester, Massachusetts 01655, and Department of Biochemistry and Cell Biology, Rice University, Houston, Texas 77025

Received May 23, 2001; Revised Manuscript Received September 24, 2001

ABSTRACT: Cooperative ligand binding in the dimeric hemoglobin from the blood clam *Scapharca inaequivalvis* results primarily from tertiary, rather than quaternary, structural changes. Ligand binding is coupled with conformational changes of key residues, including Phe 97, which is extruded from the proximal heme pocket, and the heme group, which moves deeper into the heme pocket. We have tested the role of the heme movement in cooperative function by mutating Ile 114, at the base of the heme pocket. Replacement of this residue with a Met did not disturb the hemoglobin structure or significantly alter equilibrium ligand binding properties. In contrast, substitution with a Phe at position 114 inhibits the ligand-linked movement of the heme group, and substantially reduces oxygen affinity and cooperativity. As the extent of heme movement to the normal position of the ligated state is diminished, Phe 97 is inhibited from its movement into the interface upon ligand binding. These results indicate a tight coupling between these two key cooperative transitions and suggest that the heme movement may be an obligatory trigger for expulsion of Phe 97 from the heme pocket.

The dimeric hemoglobin (HbI)[1] found in the blood clam *Scapharca inaequivalvis* is a particularly useful model system for investigating allosteric protein functions such as cooperative ligand binding. Equilibrium (*1*, *2*) and kinetic measurements (*3*, *4*) of ligand binding show clear evidence of cooperativity within this dimer, which exhibits a Hill coefficient of 1.5 for oxygen binding. Crystallographic analysis shows that although the tertiary structure of the HbI subunit is similar to that of each subunit from mammalian hemoglobins, the dimer is quite differently assembled (*5*). The HbI dimer is formed by apposition of the E and F helices, which brings the heme groups into close proximity. This arrangement allows for a more direct route for communication in HbI than in the well-known mammalian hemoglobins.

The structural transitions that underlie cooperative ligand binding in *Scapharca* HbI have been determined from crystal structures at high resolution (1.4−1.7 Å) in deoxy, CO-ligated, and oxygenated states (*5*, *6*). Comparison of these structures shows that ligand binding is coupled with localized structural changes at the dimer interface in the absence of large quaternary structural rearrangements. The absence of major ligand-linked quaternary rearrangements is dramatically illustrated by the observation that full cooperativity can be exhibited within the crystalline state (*7*).

A key role in cooperative ligand binding appears to be played by Phe 97, the side chain of which packs in the heme pocket in the deoxy form but moves into the interface upon ligand binding. This residue is thought to reduce ligand affinity when packed against the proximal side of the heme in the deoxy state by sterically restricting movement of the iron into the heme plane and lengthening a hydrogen bond involving the proximal histidine. Both of these effects can contribute to lowering the reactivity of the heme iron for binding oxygen. The contribution of Phe 97 has been probed by mutagenesis of Phe 97 to Leu (*8*), Tyr, Ala, and Val (J. E. Knapp, W. E. Royer, Jr., and M. Bonham, unpublished results). Structural and functional analyses of these mutants indicate that the degree of increased oxygen affinity, ranging from 10- to 100-fold greater than that of the wild type, is largely dependent upon the size and disposition of the residue at position 97. In all mutants of Phe 97, cooperativity is attenuated, which is consistent with the proposed role of this residue in triggering the communication between subunits that is mediated by interface water molecules (*9*). Residual cooperativity ($n \sim 1.1-1.2$) is present in these mutants, suggesting an additional route for intersubunit communication that remains in the absence of a Phe at position 97.

A plausible mechanism for such supplemental communication involves the movement of the heme groups upon ligand binding. In the absence of ligand, the heme is positioned such that the ligand binding could be sterically hindered. Binding of oxygen is coupled with a movement

† This work was supported by grants from the NIH to W.E.R. (DK43323) and Q.H.G. (GM35649), and by a postdoctoral fellowship from the New England Affiliate of the American Heart Association to J.E.K.

* To whom correspondence should be addressed. Telephone: (508) 856-6912. Fax: (508) 856-6231. E-mail: william.royer@umassmed.edu.

‡ University of Massachusetts Medical School.

§ Rice University.

[1] Abbreviations: Hb, hemoglobin; HbI, hemoglobin I; *n*, Hill coefficient; p_{50}, partial pressure in Torr at which 50% of the ligand binding sites are occupied; rms, root-mean-square.

10.1021/bi011071t CCC: $20.00
Published on Web 11/10/2001

of the heme deeper into the subunit, promoting more optimal geometry for ligand binding at the distal site. The involvement of the heme propionate groups in the subunit interface provides a structural pathway for intersubunit communication resulting from the observed ligand-linked heme movement. In this paper, we present results from mutations of Ile 114, which is located at the base of the heme pocket. Mutation of Ile 114 to the larger residues, Met and Phe, was performed to eliminate, or attenuate, heme transitions. A reduced level of ligand-linked heme movement is found in the Phe 114 mutant, which also reveals a close coupling between the ligand-linked heme and Phe 97 movements. These results suggest that the observed heme movement is a key trigger for cooperativity in *Scapharca* dimeric hemoglobin.

EXPERIMENTAL PROCEDURES

Site-Directed Mutagenesis, Expression, and Purification. The I114M and I114F mutations were separately introduced into the recombinant HbI gene encoded by the plasmid pCS26 (*10*) using PCR mutagenesis with one pair of complementary pairs of oligonucleotides encoding the I114M mutation (5′-CCGCTGCTGAATTCGGTAAAATGAACG-GTCCGATC-3′ and 5′-GATCGGACCGTTCATTTTAC-CGAATTCAGCAGCGG-3′) and a second pair encoding the I114F mutation (5′-CCGCTGCTGAATTCGGTAAATT-CAACGGTCCGATC-3′ and 5′-GATCGGACCGTTGAATT-TACCGAATTCAGCAGCGG-3′). The products of this reaction were used to transform *Escherichia coli* XL-Blue cells and plated on LB−agarose plates with 0.27 mM ampicillin. Plasmid DNA was isolated, and sequenced at the Nucleic Acid Facility located at the University of Massachusetts Medical School. Plasmid DNAs encoding the I114M and I114F mutations were used to transform *E. coli* strain W3110*lac***I***q* L8. Each mutant was overexpressed in a 12 L fermentor and purified as described previously (*10*).

Oxygen Binding and Kinetic Analysis. Equilibrium oxygen binding measurements were taken with tonometric methods at pH 7.2, between 24 and 25 °C, and a Hb concentration of 50 μM heme as described previously (*9*). Absorbance values for each step of oxygen addition were monitored at nine different wavelengths in the visible range. The measured absorbance differences were used for a Hill plot analysis, from which the p_{50} and Hill coefficient were determined. A reducing enzyme system was used to maintain the redox state of HbI (*11*). All measurements were carried out in triplicate. Oxygen affinities are given in terms of the partial pressure in which 50% of the ligand-binding sites are occupied (p_{50}), and the cooperativity is expressed in terms of the Hill coefficient *n*.

The ligand binding kinetics of each mutant were measured after flash photolysis by a 9 ns pulse at 532 nm from a Q-switched frequency-doubled YAG laser as described by Scott and Gibson (*12*). The bimolecular rebinding was monitored at millisecond and slower time scales, and was followed by directly sampling the output from a photomultiplier and fast operational amplifier with the DAS50 A/D converter. In later experiments, a Tektronix digital oscilloscope (2 gs/s maximum rate, 8 bit resolution) replaced the A/D converter. Averaging was continued until a visually satisfactory signal/noise ratio had been achieved. For each mutant, data were collected on a sample equilibrated with 1 atm of O_2, and with either 10% CO in N_2 or 1 atm of CO, and sometimes with both. Several levels of photolysis were used with each ligand, in the case of CO, 7−10 levels covering a range of photolysis from 0.99 to ≤0.05. In these experiments, the observing wavelength was 436 nm. Additional information about oxygen binding and release was obtained by equilibrating samples with 10% CO containing 2−6% O_2. Following photolysis of CO, oxygen binds rapidly. Bound oxygen then dissociates and is replaced by CO. For these experiments, an observing wavelength of 410 nm was used, which is near the COHb−Hb isosbestic wavelength.

The O_2 and CO binding data were first treated as the result of simple second-order reactions, though, in general, the CO binding rate varies systematically with the level of photolysis, and the time course of binding at a single photolysis level is not always accurately second-order. Further analysis used a kinetic equivalent of the two-state model of Monod et al. (*13*), assuming equilibrium of the R and T states. The equations may be written in terms of the allosteric constant *c*, the ratio of the affinities of the R and T state molecules, and *L*, the equilibrium constant between the two states:

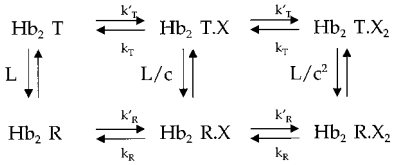

where k' represents a combination constant and k represents a dissociation rate constant. The observed rates of binding and dissociation do not reflect the properties of a single molecular species; they are the sum of the R and T rates weighted by the concentration of each species. These equations, though simple in principle, are difficult to apply in practice because *L* and *c* are highly correlated. The R and T species are assumed to be in equilibrium because (1) control experiments with different concentrations of ligand and comparison of stopped flow and flash photolysis experiments with CO have shown no evidence of slow interconversion between the R and T species and (2) the structures exhibit minimal quaternary change on ligand binding to HbI (*5*).

To apply the model to kinetics, a series of equations of the form

$$-\mathrm{d}[\mathrm{Hb}_2]/\mathrm{d}t = 2(f_\mathrm{T}k'_\mathrm{T} + f_\mathrm{R}k'_\mathrm{R})[\mathrm{Hb}_2][\mathrm{O}_2] - (f_\mathrm{T}k_\mathrm{T} + f_\mathrm{R}k_\mathrm{R})[\mathrm{Hb}_2\mathrm{O}_2] \quad (1)$$

where f_T and f_R are the fractional populations of the T and R forms, respectively, calculated from *L* and *c*. Analogous expressions were used for CO and the mixed O_2/CO molecule, required for experiments with both ligands together. Numerical solutions were compared with data using a nonlinear least-squares program. Data were included in each run for oxygen and CO alone with five to seven levels of photolysis for CO, and three levels of oxygen for the replacement reactions, as well as the equilibrium curve. Starting values for the parameters being varied were supplied by a random number generator, and at least 50 different starting points were used.

Crystallization and X-ray Diffraction Analysis. Both the CO-ligated and deoxy forms of I114M grew under the

Table 1: Statistics for the Refined Models of I114M and I114F, both in the Presence and in the Absence of CO

	I114M-CO	deoxy-I114M	I114F-CO	deoxy-I114F
resolution range (Å)	40.0−1.5	40.0−1.9	40.0−2.1	40.0−2.2
high-resolution bin (Å)	1.55−1.5	1.97−1.9	2.18−2.1	40.0−2.2
completeness[a]	88.1 (39.9)	94.8 (81.7)	88.6 (78.5)	97.2 (81.4)
$I/(\sigma I)$[a]	14.7 (2.6)	14.5 (2.9)	8.6 (3.9)	14.0 (6.9)
R_{merge}[a]	0.066 (0.235)	0.069 (0.256)	0.092 (0.215)	0.093 (0.173)
multiplicity	3.0	2.2	2.2	3.8
total no. of reflections ($F > 1\sigma$)	40765	22491	30296	27408
no. of reflections in the R_{free} test set	4098	1773	3036	1410
R-factor	0.212	0.171	0.211	0.179
R_{free}	0.235	0.201	0.247	0.214
no. of non-hydrogen atoms				
protein atoms	2322	2232	4476	4476
heme and ligand atoms	90	86	180	172
solvent molecules	165	151	149	228
average *B*-factors (Å^2)				
main chain atoms	17.2	15.1	17.6	19.6
side chain atoms	17.3	19.6	23.9	26.7
heme atoms	14.1	13.2	23.0	24.0
CO ligands	13.9	−	28.3	−
solvent atoms	29.8	30.2	29.0	34.0
rms deviations from ideal values				
bond lengths (Å)	0.007	0.006	0.005	0.007
bond angles (deg)	1.10	1.28	1.00	1.39
dihedral angles (deg)	19.0	18.2	18.0	18.1
improper angles (deg)	1.12	1.20	0.99	1.07
Ramachandran plot (%)				
most favored regions	94.7	94.3	93.7	94.5
allowed regions	5.3	5.7	6.3	5.5

[a] Values in parentheses represent the statistics calculated for the highest-resolution shell.

conditions used to crystallize the corresponding form of wild-type HbI (*5*). Crystals of the deoxy and CO-ligated forms of I114M are isomorphous to those of wild-type HbI grown in the corresponding state. Crystals of I114M-CO belong to the *C*2 space group, include one intact dimer per asymmetric unit, and have the following cell dimensions: $a = 93.1$ Å, $b = 44.0$ Å, $c = 83.4$. Å, and $\beta = 122.0°$. Crystals of deoxy-I114M belong to the $C222_1$ space group and have an intact dimer per asymmetric unit with the following cell dimensions: $a = 91.8$ Å, $b = 44.5$ Å, and $c = 143.9$ Å.

I114F-CO crystallized under the same conditions used to grow crystals of CO-ligated HbI. However, the analysis of the data showed that these crystals belong to the $P2_1$ space group and have the following cell dimensions: $a = 83.7$ Å, $b = 44.1$ Å, $c = 87.3$ Å, and $\beta = 115.4°$. The asymmetric unit of the $P2_1$ crystal form includes two intact dimers. (This $P2_1$ crystal form is related to the *C*2 crystal form observed in HbI-CO crystals, with the $P2_1$ *a* axis in the direction of the *C*2 *c* axis, the *b* axes coincident in the two crystal forms, and the $P2_1$ *c* axis along the $-ac$ diagonal of the *C*2 cell. The packing between molecules is similar in both crystal forms.)

The deoxy form of I114F did not form crystals under the conditions used to crystallize wild-type deoxy-HbI. A deoxy-I114F structure was obtained by transforming CO-ligated crystals into the unligated state. The CO-ligated Hb in I114F crystals was first converted to the cyanomet form by soaking these crystals in 150 mM potassium ferricyanide, 300 mM potassium cyanide, and 2.2 M phosphate (pH 7.5) for 2 h. This soak took place at room temperature and under a lamp. The crystals were then rinsed in a stabilizing solution of 2.2 M phosphate (pH 7.5) and transferred into an anaerobic chamber (Anaerobe Systems, Morgan Hill, CA). The crystals were then reduced in the anaerobic chamber by soaking in 150 mM sodium dithionite and 2.2 M phosphate (pH 7.5) for 2 h. [A similar procedure can be used to convert the wild-type HbI−CO crystals into a fully deoxy form that shows all the structural attributes of deoxy-HbI observed in crystals grown in the deoxy state (J. E. Knapp, unpublished observation).] These crystals retained the $P2_1$ space group symmetry, with the following cell dimensions: $a = 83.7$ Å, $b = 44.2$ Å, $c = 87.2$ Å, and $\beta = 115.5°$.

All X-ray data sets were collected with an R-AXIS IIC image plate detector mounted on a Rigaku II generator equipped with mirror optics (Molecular Structure Corp., The Woodlands, TX). The I114M-CO data set was collected from a single crystal using crystal to film distances of 60 and 65 mm, an oscillation angle of 1.2°, and an exposure time of 12 min per image. The I114F-CO data set was obtained from two crystals, using crystal to film distances of 65 and 80 mm, an oscillation angle of 1.2°, and an exposure time of 12 min. The deoxy-I114M and deoxy-I114F data sets were both collected from single crystals using crystal to film distances of 95 and 120 mm, oscillation angles of 1.0° and 1.6°, and image exposure times of 12 and 10 min, respectively. X-ray data for each data set were processed and merged using the HKL package (*14*). The data collection statistics are displayed in Table 1. All four data sets are more than 88% complete to their resolution limits. It should be noted that the effective resolution for the I114M-CO data set is 1.6 Å because of the lack of completeness in the outer shell. However, data to 1.5 Å resolution were included in the refinement of this structure.

Phasing and Refinement. The starting phases were obtained using wild-type HbI-CO (*5*) and wild-type deoxy-HbI (*5*) as the initial models. The side chains of position 114 were truncated to an alanine before phasing. Crystals of I114F-CO and deoxy-I114F are not isomorphous to wild-

type HbI crystals and required molecular replacement calculations to position the starting model. The program EPMR (*15*) found four solutions within the I114F-CO asymmetric unit when one subunit of the HbI-CO structure was used as the search model. The deoxy-I114F crystals are isomorphous to those of I114F-CO, which allowed us to calculate initial phases with the refined model.

Each model was subjected to two rounds of CNS refinement (*16*) sandwiched around a manual fitting. Bulk solvent corrections were included throughout refinement (*17*). The first round of refinement included overall *B*-factor refinement, maximum likelihood, conjugate gradient energy minimization, and *B*-factor refinement. Water molecules were then added to the model using the water pick procedure of CNS (*16*). Each water molecule was retained in the model if density was present in an omit, $2F_o - F_c$ sigmaA weighted electron density map (*18*) contoured at 1.0σ and if it had reasonable hydrogen bonding partners. The last round of the refinement of the two I114M structures included energy minimization and individual *B*-factor refinement. The last round of refinement of the two I114F structures included the refinement of a main chain and side chain *B*-factor for each residue. The last round of the I114F-CO refinement included a simulated annealing step.

Superposition calculations were carried out with the program LSQMAN (*19*). Calculation of a least-squares plane through heme atoms was carried out with the program Geomcalc of the CCP4 package (*20*). The atomic models and diffraction data for deoxy and CO forms of I114M and I114F have been deposited in the Protein Data Bank (*21*), as entries 1JWN, 1JZK, 1JZL, and 1JZM.

RESULTS

Equilibrium and Kinetic Ligand Binding Properties. Wild-type HbI binds oxygen cooperatively, with measured p_{50} values between 10.0 and 10.6 Torr and Hill coefficients (n) between 1.41 and 1.53 at 24 °C. The substitution of a Met at position 114 results in a minimal change in oxygen affinity (p_{50} between 9.0 and 9.8 Torr) and maintains full cooperativity (n between 1.42 and 1.51) under the same experimental conditions. In contrast, substitution of a Phe at position 114 results in a >2-fold drop in affinity (p_{50} between 20.4 and 21.3 Torr) and a sharp loss in cooperative oxygen binding (n between 1.04 and 1.12). These are the lowest Hill coefficients measured for any mutant of HbI analyzed to date, indicating a severe disruption of the cooperative mechanism.

Kinetic analysis carried out within the context of a two-state model (*13*) is consistent with these conclusions. Experiments on CO binding at different levels of photolysis (Figure 1) provide an indication of the R−T equilibrium in the Hb_2 and Hb_2CO species with Hb_2 predominant at high levels of photolysis and Hb_2CO at low levels of photolysis. (Hb_2 designates an unligated hemoglobin dimer, while Hb_2-CO designates a dimer that is singly ligated with CO.) The results show that there is a greater proportion of the R state in wild-type Hb_2CO than in Hb_2. This can be roughly quantified by using the estimate of Pardanani et al. (*8*) that binding to the R state is 30 times faster than binding to the T state. The observed increase in rate is 50%, calling for an R state population of some 2%. The change in the rate for I114M is about half as great, and in I114F no change is observed, suggesting that Hb_2CO remains almost entirely in the T state in I114F.

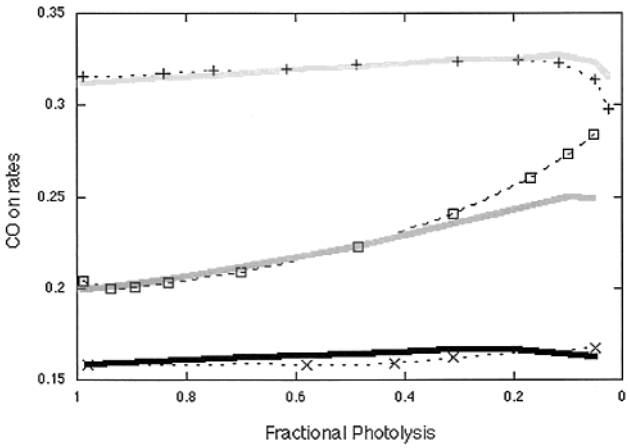

FIGURE 1: CO combination rates for I114M (+), the wild type (□), and I114F (×) are plotted as a function of fractional photolysis. Note how the low flash measurements (toward the right) for the wild type, which should primarily measure the level of ligand binding to singly ligated HbI, result in higher combination rates than under nearly complete flash photolysis, for which binding will primarily be to deoxy-HbI. This increase in combination rates as the extent of photolysis is decreased is indicative of cooperativity. For I114F, there is no change in the rate with the extent of photolysis, while there is only a small change with I114M. The CO on rates for I114M are slightly faster than those of the wild type, and I114F on rates are slightly slower. The continuous lines show the output of application of a two-state model for such data on these mutants.

Experiments with high concentrations of oxygen yield information about the Hb_2O_2 species only, as the combination of a lower quantum yield and a large nanosecond geminate reaction, typically 50% under our experimental conditions, allow photolysis of only a small proportion of combined oxygen. The rates were as follows: 16×10^6 M^{-1} s^{-1} for the wild type, 8×10^6 M^{-1} s^{-1} for I114M, and 3.3×10^6 M^{-1} s^{-1} for I114F. The trend in rate between mutants is in the same direction as that with CO, but the proportions are different. It is believed that in myoglobin the rate of the oxygen reaction at the heme is hundreds of times faster than that with CO, and that the bimolecular rate of the reaction with oxygen is limited by diffusion within the molecule (*22*). Similar considerations have been shown to apply to HbI (J. S. Olson, W. E. Royer, Jr., J. E. Knapp, Q. H. Gibson, unpublished experiments). In contrast, in the CO reaction, the rate of reaction at the heme is limiting, diffusion has minimal effects, and the geminate reaction is small in magnitude. Accordingly, the low rate of oxygen binding in I114F is consistent with Phe obstructing entry of oxygen into the heme pocket, and with residue 114 being on the normal pathway for diffusion of oxygen into the heme pocket.

Data from experiments with low concentrations of oxygen (Figure 2) add further information. The starting point in these experiments is $Hb_2(CO)_2$. Immediately after photolysis, the predominant species is Hb_2 which reacts faster with oxygen than with CO. The rate of the approach to equilibrium with oxygen is given by the sum of the on and off rates (eq 1), and the amplitude of the reaction is determined by their ratio. Estimates of both rates have been made by deconvolution of the traces (Figure 2, left panel). The full model is required

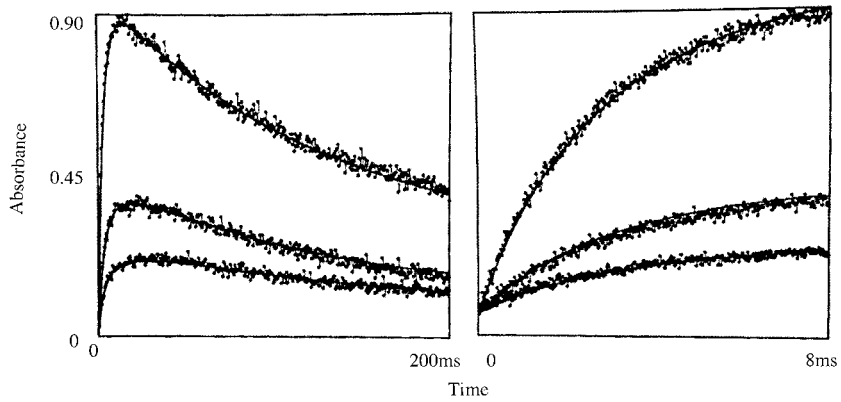

FIGURE 2: O_2/CO replacement kinetics on I114F. Each curve is the observed data from samples of I114F equilibrated with 10% CO along with 11.8 (bottom), 23.5, and 71 μM O_2. The full reaction following a laser flash is followed for 200 ms (left), and the progress of the reaction during the first 8 ms is shown at the right. Both the combination rate of O_2 with I114F (right) and the rate of its subsequent replacement by CO (left) were fitted by least squares to a two-state model. The CO replacement reaction is dependent upon the oxygen off rate. The least-squares fit gives an O_2 off rate of 94 s^{-1}. The O_2 on rate was 3.5×10^6 M^{-1} s^{-1}.

to take account of the changing concentrations of the various species and changing R and T proportions as the reaction proceeds. For the wild type, k'_T is 10×10^6 M^{-1} s^{-1} and k_T 400 s^{-1}. The corresponding figures for I114F are 3.3×10^6 M^{-1} s^{-1} and 94 s^{-1}; thus, both on and off rates for the mutant are slower, as would be expected for a diffusive effect. In summary, kinetic analysis suggests that I114F remains in the T state at all stages of ligation. It is therefore impossible to obtain data for the R state as it does not contribute to the observable behavior of the mutant.

The rate of oxygen dissociation from I114F, obtained by deconvolution of the data shown in Figure 2, is 94 s^{-1}, or approximately one-quarter of the rate reported for the wild type. The amplitude of the oxygen nanosecond geminate reaction is one of the largest so far seen at 57% as compared with 41%, the amplitude for wild-type HbI. Both of these results are also compatible with a limitation in the rate of diffusion away from the iron, with the large-magnitude geminate reaction being due to the inability of the dissociated ligand to escape along its normal pathway.

Treatment of the kinetic data for I114M using the two-state model gave excellent fits; two levels of photolysis with high oxygen levels and six data sets for the replacement reaction together with four levels of photolysis for CO and the equilibrium curve data yielded an rms residual of 0.0028 in absorbance. Although the mutant I114M resembles the wild type fairly closely, the results suggest that the T state is favored more than in the wild type and that there is some hindrance to diffusion of ligands into and out of the protein reflected in the lower rate of oxygen binding and in the lower rate of dissociation of oxygen from the T state (330 vs 400 for the wild type). The retention of T state behavior at higher fractional saturation accounts for the smaller change in the rate of CO binding at the low level of fractional photolysis shown in Figure 1.

Crystal Structures of I114M. Crystals of the CO-ligated and unligated forms of I114M are isomorphous to wild-type HbI, showing the symmetry of space groups $C2$ and $C222_1$, respectively. The atomic model for I114M-CO has been refined to a limiting resolution of 1.6 Å (but including some data to 1.5 Å) and an R-factor of 0.212 ($R_{free} = 0.235$), while the unligated I114M structure has been refined at 1.9 Å resolution to an R-factor of 0.171 ($R_{free} = 0.201$). Model statistics are provided in Table 1. Electron density maps show clear density for the methionine side chain at position 114. This residue assumes different conformations in the two subunits of the asymmetric unit, indicating its flexibility. Met 114 fits into a hydrophobic pocket on the distal side of the heme, forming favorable contacts with the side chains of Leu 36, Met 37, Leu 40, and Pro 117. The side chain of Met 114 also interacts with the heme, with atoms within van der Waals distances of the ethylene group from the B ring, with the methyl group of the C ring, and with the B−C bridging methylene carbon. The side chain is positioned so that Cϵ is between 4.1 and 4.3 Å from the oxygen from the CO ligand.

The introduction of a Met at position 114 does not alter the overall structures of either the ligated or unligated forms. Superposition of 137 Cα atoms from each subunit of CO and deoxy-I114M upon their wild-type counterparts gives average rms differences of 0.077 ± 0.001 and 0.081 ± 0.001 Å, respectively. Met 114 also does not significantly alter the position of the heme group in either state (Figure 3). The distance between the heme irons from two adjacent subunits within the unligated forms of both HbI and I114M is 16.6 Å, whereas this distance is 18.4 and 18.5 Å for the CO-ligated forms of HbI and I114M, respectively. Phe 97, a key residue implicated in the cooperative function, packs against the heme in the absence of ligand, and moves to the interface upon ligand binding (Figure 3). The dimer interfaces of each form of I114M remain identical with those of wild-type HbI, in the corresponding ligation state. This similarity extends to the presence of 11 and 17 ordered core water molecules, respectively, in the interfaces of the CO-ligated and unligated forms of I114M.

Crystal Structures of I114F. While crystals of previous HbI mutants have been isomorphous to HbI crystals of the corresponding ligand state, crystals of I114F-CO grew in a new lattice. These crystals show the symmetry of space group $P2_1$, with two dimers per asymmetric unit. The molecular packing in these crystals is similar to that in the wild-type crystal form, whose C-centered lattice has only a single dimer per asymmetric unit. The atomic model for I114F-CO refined to an R-factor of 0.211 ($R_{free} = 0.247$) at 2.1 Å resolution while maintaining good stereochemistry (Table 1). Crystals of deoxy-I114F are isomorphous with those of I114F-CO.

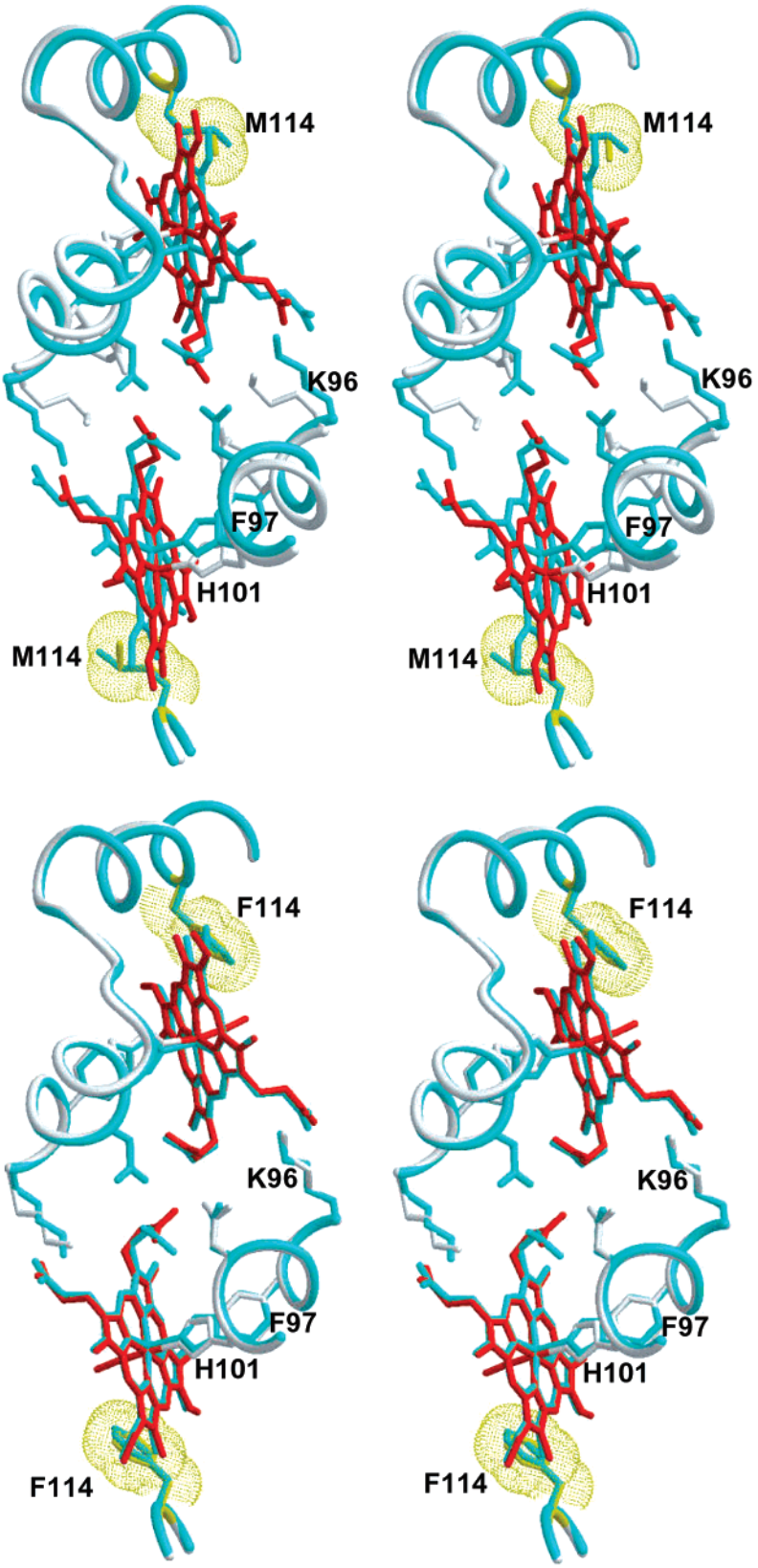

FIGURE 3: Structural transitions between the CO-ligated and deoxy forms of I114M (top) and I114F (bottom). Deoxy structures are shown in cyan, whereas the CO hemes are shown in red; residue 114 is shown in yellow with the rest of the structure in gray. A van der Waals surface is shown for the side chains of residue 114. The main chain trace from the middle of helix F into helix G is shown in the top subunit for each dimer. The heme groups of I114M display a large ligand-linked movement, comparable to what is seen in the wild type, which is consistent with its full cooperativity. The level of movement of the heme groups within I114F is dramatically reduced, resulting in a number of changes that reduce the cooperative ligand binding properties of this mutant. This figure was prepared with the program MIDAS (*29*).

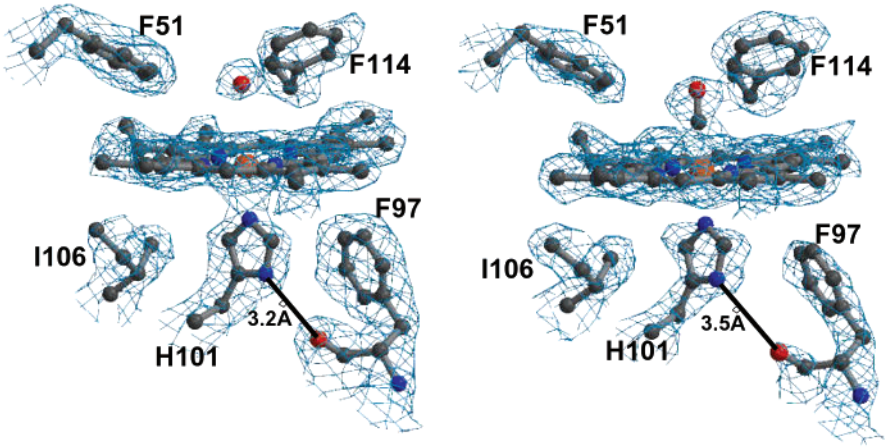

FIGURE 4: Heme pockets of the unligated (left) and CO-ligated (right) forms of I114F. SigmaA weighted, $2F_o - F_c$, simulated annealing omit maps are superimposed upon the refined models. The electron density around the deoxy heme omitted residue 114 from the calculations, whereas the density around the CO-ligated heme pocket omitted residue 97. There is little change in the position of Phe 97 between these two structures. Also note the distances between the carbonyl oxygen of Phe 97 and Nδ2 of His 101. This figure was prepared with the computer program BOBSCRIPT (*30*) followed by raster rendering by RASTER3D (*31*).

This atomic model refined to an *R*-factor of 0.179 (R_{free} = 0.214) to 2.2 Å resolution, also while maintaining good stereochemistry.

The introduction of a phenylalanine at position 114 only slightly alters the structure of deoxy-I114F compared to the deoxy wild type, but significantly alters the structure of the CO-ligated state. The four subunits within the I114F-CO asymmetric unit superimpose onto their counterparts from HbI-CO and deoxy-HbI with rms distances of 0.34 ± 0.06 and 0.25 ± 0.04 Å, respectively, for 137 Cα atoms (residues 10−146). Similarly, the four subunits of deoxy-I114F (137 Cα atoms) superimpose onto the corresponding atoms of the ligated and unligated HbI coordinates with rms distances of 0.35 ± 0.03 and 0.21 ± 0.04 Å, respectively. Clearly, the overall structure of I114F-CO exhibits a number of structural properties that are more similar to those of the deoxy form than those of the ligated forms of HbI. Specifically, these changes are localized to the position of the heme group, the conformation of Phe 97, and the residues that form the subunit interface, as well as small changes in the quaternary structure (Figure 3).

The simulated annealing omit electron density from a $2F_o - F_c$, sigmaA weighted map shows clear density for the phenylalanine side chain at position 114 (Figure 4). The phenylalanine assumes an orientation χ_1 (Cα−Cβ torsion angle) of −138 ± 11° and χ_2 (Cβ−Cγ torsion angle) of 83 ± 1°, placing the ring so that it is pointing toward Leu 73 and Met 37, and near the vinyl group attached to the B pyrrole ring of the heme. The side chain of I114F, like I114M, fits into a hydrophobic pocket, forming a number of favorable contacts with Leu 36, Met 37, Leu 40, and Leu 73. The Phe side chain packs tightly against the heme group, forming more extensive contacts with the heme than I114M. The binding of the ligand does not significantly alter the χ_1 angle, but does result in a 10° rotation about the χ_2 angle (χ_2 = 73 ± 3°). This slight rotation appears to follow the ligand-linked movement of the heme group, and moves the side chain so that it is between 4.6 and 5.0 Å from the CO ligand.

Ligand-Linked Movements of Phe 97 and the Heme Group. Phe 114 forms a number of van der Waals contacts with the distal face of the heme group, sterically restricting the heme group from moving as deeply into the heme pocket as in HbI-CO. This is seen by the superposition of the Cα atoms (residues 10−146) of I114F-CO onto the corresponding atoms of HbI-CO (Figure 5). The heme group has pivoted down (using the orientation in Figure 5) from Phe 114 and up from Phe 97. This translates the heme iron by 0.4 ± 0.2 Å toward the interface relative to HbI-CO. This positions the I114F-CO hemes such that the distance between the heme irons is 17.4 Å for the A−B dimer and 17.8 Å for the C−D dimer. In contrast, the distance between heme irons is 18.4 Å in HbI-CO and 16.6 Å in both deoxy-HbI and deoxy-I114M. The I114F mutation also alters, to a much lesser extent, the position of the heme group in the deoxy state. The superposition of the Cα atoms of deoxy-I114F (residues 10−146) onto the corresponding atoms of deoxy-HbI

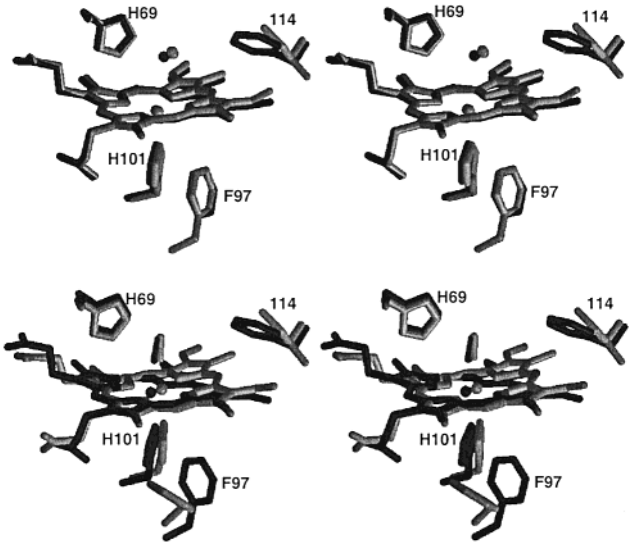

FIGURE 5: Superposition of the A subunit from the wild type (gray) onto that of I114F (black). This superposition included the Cα atoms from residues 10−146, and was repeated for both the unligated (top) and CO-ligated forms (bottom) of each Hb. The comparison of I114F-CO with HbI-CO shows that the heme group pivots and translates away from Phe 114 and pivots up above Phe 97. This figure was prepared with Molscript followed by RASTER3D (*31*).

Table 2: Heme Geometry in the Refined Atomic Models

	WT-CO[b]	I114M-CO	I114F-CO	deoxy-WT	deoxy-I114M	deoxy-I114F
Fe−Np plane	0.012	0.009	0.005	0.359	0.352	0.247
Fe−heme plane[a]	0.039	0.027	0.10	0.519	0.513	0.359
Fe−Np (avg)	2.013	2.013	2.020	2.035	2.005	2.032
Fe−Nϵ2 (His 101)	2.069	2.048	2.073	2.075	2.038	2.060
Fe−C (CO)	1.860	1.84	1.89	–	–	–
Fe−C−O (CO)	172.5	174.9	174.7	–	–	–
O (CO)−Nδ2 (69)	2.81	2.88	2.75	–	–	–
Phe 97 O−Nδ1	2.83	2.89	3.57	3.12	3.21	3.26
A Fe−Fe B	18.4	18.5	17.6	16.6	16.6	16.9

[a] Defined as the plane formed by the pyrrole rings and the bridging methylene carbons. [b] These numbers represent a model that was refined under the same conditions that were used for the two I114 mutants, using CNS (*16*).

indicates that the heme group has shifted 0.18 ± 0.05 Å away from the interface. The distances between the iron atoms from adjacent hemes are 16.9 Å for both the A−B and C−D dimers. Thus, the average movement of the heme iron between ligated and unligated states is attenuated from 0.77 ± 0.04 Å as observed in the wild type to 0.35 ± 0.09 Å in I114F.

A significant, and unexpected, result in the I114F-CO structure concerns the disposition of Phe 97. This residue is located on the proximal side of the heme, and more than 8 Å away from Phe 114. The Phe 97 side chain in deoxy-I114F packs against the heme group, like wild-type HbI. However, the binding of ligand does not alter the position of Phe 97 as it does in HbI. Rather, Phe 97 remains packed against the heme in the CO-ligated structure, whereas this side chain moves into the interface in both wild-type HbI and I114M upon ligation. Accommodation of Phe 97 in the heme pocket of I114F-CO requires a slight reorientation of the heme group, which pivots away from Phe 97 by ~0.4 Å, thereby removing steric clashes that would prohibit Phe 97 from occupying its T state conformation.

There does appear to be a small conformational change of Phe 97 that is linked to ligand binding. In three of the four subunits of I114F-CO, Phe 97 has χ_1 angles of 164 ± 4° and χ_2 angles of 76 ± 4°. Phe 97 in the fourth (C) subunit has a χ_1 angle of 162° and a χ_2 angle of 103°. The χ_1 and χ_2 angles of all four subunits change to 169 ± 2° and 85.3 ± 0.5 °, respectively, in the absence of ligand. The position of Phe 97 in three of the four subunits within this mutant HbI introduces strain into the proximal histidine−heme iron bond that would lower the ligand affinity of the R state form of this Hb. The small but significant rotation of the heme ring could relieve this strain and account for the small residual cooperativity observed in the oxygen equilibrium experiments. The conformation of the lone outlier, Phe 97 from the C subunit in the CO-ligated state, is poorly defined in density, suggesting that this residue is partially disordered.

These changes have important effects upon the ligand-binding site of this mutant (Table 2). The heme iron of I114F-CO lies within the plane of the heme group, but moves 0.36 ± 0.03 Å out of the plane in the absence of ligand. This distance is significantly shorter than that observed in wild-type HbI or I114M (0.52 ± 0.02 Å). Despite this change, the length of the bond between the heme iron and Nϵ of the proximal histidine is similar to that of the wild type (2.060 ± 0.008 Å in deoxy-I114F vs 2.075 ± 0.005 Å in HbI). Possibly, the structural effect in the proximal pocket that would most directly impact oxygen affinity in I114F is a hydrogen bond between proximal His Nδ and the carbonyl oxygen of Phe 97. This hydrogen bond has previously been suggested to contribute to regulation of oxygen affinity in HbI, because the stronger hydrogen bond observed in the ligated form could help stabilize bound oxygen (*5*). In the deoxy forms of I114M, I114F, and wild-type HbI, long (3.2 Å) hydrogen bonds are formed, which shorten to between 2.8 and 2.9 Å upon ligation of I114M and wild-type HbI. However, the distance increases to >3.5 Å in I114F-CO (Figure 4), which suggests that this hydrogen bond is absent.

Dimer Interface and Quaternary Assembly. The disruption of the cooperative pathway by attenuating the normal movements of the heme groups results in an alteration of the dimer interfaces of ligated I114F. Specifically, the side chains that form the A−B dimer interface occupy conformations that are nearly identical to those occupied by their counterparts in deoxy-HbI. The lone exception is the position of propionic acid A from the B heme. This side chain would be in the deoxy conformation except for the carboxylate group, which is rotated by 90° from that of its counterpart within deoxy-HbI. The water cluster of the A−B interface exhibits a deoxy-like structure, with 16 of the 17 water molecules present in deoxy-HbI also present at this interface. Only one water molecule is absent in the A−B dimer of I114F-CO, but is present in the deoxy form of this mutant. The side chain of the A propionic acid of the B heme assumes a deoxy conformation in the absence of ligand.

The residues that form the C−D interface exhibit properties that are intermediate between those of the ligated and unligated states. Lys 96 occupies the deoxy conformation. The positions of Arg 53 and Arg 104 from both the C and D subunits occupy conformations that are between the ligated and unligated states, but closer to the unligated state. The D propionic acid side chains from both heme groups are in a T state position, whereas the propionic acid side chains from the A rings are in an R state conformation, with the carboxylate rotated by 30° with respect to its counterpart from HbI-CO. The side chain of Asn 100, which interacts with the propionic acid A from the neighboring subunit, is in a position that is between the ligated and unligated conformations, thereby maintaining its hydrogen bond with the propionic acid. The water cluster at the C−D interface is less like the cluster of deoxy-HbI, with 13 of the 17 water molecules found in deoxy-HbI also present at the C−D interface. In the absence of ligand, the C−D interface becomes essentially identical with that of deoxy-HbI. The propionic acid side chains of the two heme groups, as well as the side chains of Asn 100 from both subunits, assume

deoxy conformations. Three of the four waters missing in I114F-CO are present in the deoxy form of this mutant.

The I114F substitution and attenuation of the ligand-linked heme movements along with the changes at the subunit interface have an important impact on the quaternary structure of HbI. Unlike mammalian hemoglobins, the R to T state transition of HbI occurs with only a minimal change in the relative orientations of the two subunits. The two states differ in quaternary structure by a 3.3° rotation in wild-type HbI, but differ by only 0.5° and 0.6° in the A−B and C−D dimers of I114F, respectively. This suggests that the small quaternary change that occurs during ligand binding is needed to accommodate the ligand-linked change of the heme position.

DISCUSSION

Mutations of Ile 114, which is at the base of the heme pocket, were produced to probe the role of the ligand-linked heme movements in the cooperative mechanism of *Scapharca* HbI. The substitution of a flexible methionine at this position does not significantly alter the equilibrium allosteric properties of this mutant, but does show some change in its kinetic properties. This mutation reduces the rates of ligand entry and increases the likelihood of ligand escape when compared to those of wild-type HbI, which results in an increase in the off rate of the T state. This increase in the off rate is offset by an increase in the heme reactivity as judged by the slight increase in the CO on rates. Thus, I114M retains it ability to bind ligands in a cooperative fashion. The crystal structures of the ligated and unligated forms of this mutant clearly show that it undergoes the same ligand-linked structural transitions as the wild type. In contrast, the substitution of an inflexible Phe at position 114 alters the ability of this mutant to undergo the structural transitions during ligand binding, thereby reducing both the affinity and cooperativity. Furthermore, Phe 114 reduces the accessibility of ligands to the heme group. These combined effects account for the observed equilibrium and kinetic properties of this mutant.

The crystallographic analysis of I114F reveals that the structural basis for the loss of affinity and cooperativity is a loss of the ligand-linked heme movement observed in *Scapharca* HbI. This indicates that the observed heme movements are critical for cooperativity in *Scapharca* HbI. In fact, attenuating the heme movement in I114F results in a cooperativity that is lower than that observed with mutants of Phe 97, despite the central role of Phe 97 in regulating ligand affinity. This provides new insight into the structural basis for cooperativity in HbI. The ligand-linked heme transitions may be the central allosteric event in this dimeric hemoglobin. However, when the conformation of this Phe 97 is coupled to the heme position, the level of cooperativity can be greatly enhanced over that resulting from just the heme transitions. This is consistent with experiments in which the protoheme group of HbI is substituted with mesoheme groups. These modified Hbs also show decreases in cooperativity, while resonance Raman spectroscopy suggests that the mesoheme group is immobilized such that it cannot move to its T state position (*23*). Thus, the two alternate approaches indicate that attenuating the ligand-linked heme movement inhibits the transition between allosteric states in HbI.

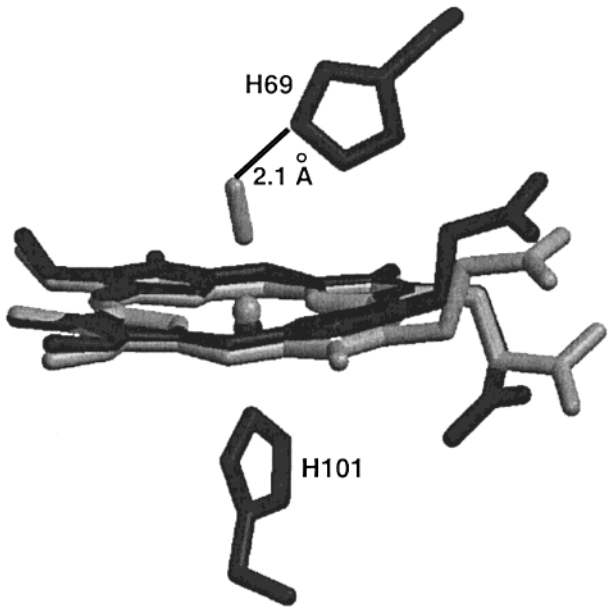

FIGURE 6: Steric hindrance of the T state distal histidine (residue 69) for ligand binding. This figure shows a CO-ligated heme (gray) manually superimposed upon the heme group from deoxy-HbI (black). This superposition minimized the differences between the four pyrrole nitrogen atoms of the two heme groups, and resulted in an rms distance of 0.08 Å for the four atoms. This positions the CO heme such that the oxygen from the CO ligand is 2.1 Å away from the Nϵ atom of His 69. This figure was prepared with Molscript followed by RASTER3D (*31*).

Distal and Proximal Contributions to the Regulation of Oxygen Affinity. Comparison of diverse hemoglobins has revealed several broad principles by which the protein stereochemistry can alter oxygen affinity (*24*). Structural changes on the proximal side of the heme can alter the chemical reactivity of the heme iron, while distal effects can either limit access of the ligand to the heme pocket or stabilize the bound ligand using neighboring residues.

Kinetic analysis of ligand binding properties can provide strong evidence for the basis of affinity modulation. Combination rate constants for oxygen and nitric oxide binding are largely determined by diffusion pathways or by the introduction of steric barriers at the ligand-binding site because the reaction of the heme iron with these ligands is not rate-limiting. The modulation of combination velocities during successive ligand binding steps appears to contribute only slightly to the cooperativity observed in oxygen equilibria of most cooperative hemoglobins, including HbI. However, cooperativity can be achieved through this type of regulation. In lamprey hemoglobin, large differences in oxygen combination rates are observed between low- and high-affinity forms because the distal histidine acts as a steric barrier in the low-affinity form (*25*, *26*). On the other hand, modulation of oxygen dissociation rates provides a major contribution to regulation of oxygen affinity of a number of cooperative hemoglobins. The significant contribution of oxygen dissociation rates requires contributions of proximal alteration of iron reactivity and/or distal stabilization of the bound ligand.

Previous work on structural aspects of the cooperative mechanism of *Scapharca* HbI has concentrated on the role of proximal effects in HbI. A key residue, Phe 97, packs against the proximal side of the heme in the deoxy state,

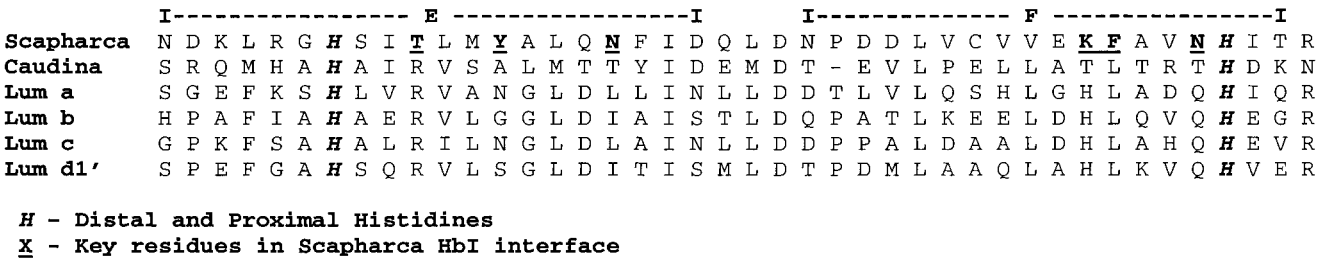

FIGURE 7: Sequence alignment of hemoglobins that assemble into E−F dimers. This alignment only includes residues between helices E and F, and includes the HbI sequence from *S. inaequivalvis* (*32*), the HbD sequence from *C. arenicola* (*33*), and the sequences from the four hemoglobin chains encoded by *L. terrestris* (*34*, *35*).

thereby restricting the movement of the heme iron to the heme plane and weakening the hydrogen bond between the carboxyl oxygen of Phe 97 and Nδ of the proximal histidine. Both of these effects could reduce the affinity of the unligated state. The binding of ligand results in the expulsion of Phe 97 into the interface, increasing the ligand affinity of the R state. The mutation of Phe 97 (*8*) results in increased ligand affinity and decreased cooperativity. Kinetic analysis shows that the difference in the off rate constants between the fully and singly ligated species is essentially lost as a result of the elimination of proximal contributions to cooperative ligand binding. Despite the loss of the proximal effects, these mutants exhibit residual cooperative ligand binding as observed both in equilibrium measurements and in differences in the on rates between the first and second steps of carbon monoxide binding. This suggests that the observed modulation of oxygen combination rates results from distal contributions to cooperativity.

In contrast to mutations of Phe 97, the substitution of a Phe at position 114 reduces both the proximal and distal contributions to cooperativity. By preventing the normal ligand-linked heme movement, Phe 114 allows Phe 97 to remain packed in the heme pocket, even in the presence of ligand. An important functional consequence of this packing is the disruption of the hydrogen bond between the proximal histidine and the carbonyl oxygen of Phe 97 in the CO-ligated state. This hydrogen bond has been implicated in contributing to the strong oxygen affinity of the R state form of HbI by stabilizing a partial positive charge on the proximal histidine that results from oxygen binding (*5*). The lack of a strong hydrogen bond in both states is likely to be responsible, at least in part, for the low affinity of I114F. By elimination of the ligand-linked transitions of Phe 97, the level of proximal modulation of oxygen affinity is severely reduced.

Distal contributions to cooperativity in HbI arise from the heme movement that brings the distal histidine and heme iron into a more favorable stereochemical arrangement for ligand binding in the R state. In the low-affinity T state, access to the heme iron appears to be sterically restricted by the distal histidine, in a manner similar to, albeit less restrictive than, that observed in deoxy lamprey Hb (*25*). This can be seen by the superposition of a ligated heme onto the deoxy-HbI heme (Figure 6), which places the ligand within 2.1 Å of the distal histidine. Thus, the binding of ligand requires that either the distal histidine or the heme group move. In the case of HbI, the heme group moves, whereas in lamprey hemoglobin, it is movements of the distal histidine that allow optimal binding of ligand (*25*, *27*). The attenuation of the ligand-linked heme movements in I114F is enough to partially reduce the steric strain of binding a ligand to the T state because the heme does not move to its fully deoxy position. The closest approach between the modeled ligand and the deoxy distal histidine is 2.4 Å in I114F. As a result, only subtle movements of the heme and distal histidine are required for ligand binding in I114F.

Coordination of the proximal and distal contributions to cooperativity in HbI results from the tight coupling of the conformation of Phe 97 with the position of the heme group. Earlier, it was proposed that these two motions are coupled because the heme movement would be triggered by the ligand-linked Phe 97 transitions (*5*). This hypothesis was refuted by analysis of the F97L mutation, which showed that the ligand-linked heme transitions occur in the absence of the Phe 97 structural transitions (*8*). The results presented here show that the ligand-linked heme and Phe 97 movements are indeed coupled; however, it is the heme movement that triggers the Phe 97 movement, rather than the reverse.

Other Cooperative Invertebrate Hemoglobins. The ability to use ligand-linked heme transitions as a mechanism for intersubunit communication in HbI arises from an assembly of subunits that involves the heme propionates in the interface. This assembly, termed an E−F dimer, has also been observed in structures of three other cooperative invertebrate hemoglobins, including the dimeric Hb from the echinoderm *Caudina arenicola*, a heterotetrameric Hb from *Scapharca* (HbII), and the giant erythrocruorin from the annelid *Lumbricus terrestris* (*24*). Interestingly, the key residues involved in the *Scapharca* HbI cooperative mechanism are not conserved in the echinoderm and annelid hemoglobin sequences (Figure 7). Most notably, Phe 97 of *Scapharca* HbI is replaced with a leucine, and Thr 72 is replaced with an arginine in the other five sequences. This suggests considerable diversity among cooperative mechanisms in E−F dimer assemblages. The central role of the heme movement in the structural transitions of HbI, as elucidated here, might be a common theme for cooperativity in these hemoglobins. Such a possibility has been suggested for the hemoglobin D from *C. arenicola* (*28*). Perhaps the heme transitions provide a low level of cooperativity in all E−F dimers and this level is supplemented by different side chain interactions, in a fashion analogous to that observed with Phe 97 in *Scapharca* HbI.

ACKNOWLEDGMENT

We thank Phyllis Spatrick of the University of Massachusetts Nucleic Acid Facility for nucleotide sequence analysis of the plasmids encoding the I114M and I114F

mutations. The contents of this paper are solely the responsibility of the authors and do not necessarily represent the official views of the NIH.

REFERENCES

1. Chiancone, E., Vecchini, P., Verzili, D., Ascoli, F., and Antonini, E. (1981) *J. Mol. Biol. 152*, 577−592.
2. Ikeda-Saito, M., Yonetani, T., Chiancone, E., Ascoli, F., Verzili, D., and Antonini, E. (1983) *J. Mol. Biol. 170*, 1009−1018.
3. Antonini, E., Ascoli, F., Brunori, M., Chiancone, E., Verzili, D., Morris, R. J., and Gibson, Q. H. (1984) *J. Biol. Chem. 259*, 6730−6738.
4. Chiancone, E., Elber, R., Royer, W. E., Jr., Regan, R., and Gibson, Q. H. (1993) *J. Biol. Chem. 268*, 5711−5718.
5. Royer, W. E., Jr. (1994) *J. Mol. Biol. 235*, 657−681.
6. Condon, P. J., and Royer, W. E., Jr. (1994) *J. Biol. Chem. 269*, 25259−25267.
7. Mozzarelli, A., Bettati, S., Rivetti, C., Rossi, G. L., Colotti, G., and Chiancone, E. (1996) *J. Biol. Chem. 271*, 3627−3632.
8. Pardanani, A., Gibson, Q. H., Colotti, G., and Royer, W. E., Jr. (1997) *J. Biol. Chem. 272*, 13171−13179.
9. Royer, W. E., Jr., Pardanani, A., Gibson, Q. H., Peterson, E. S., and Friedman, J. M. (1996) *Proc. Natl. Acad. Sci. U.S.A. 93*, 14526−14531.
10. Summerford, C. M., Pardanani, A., Betts, A. H., Poteete, A. R., Colotti, G., and Royer, W. E., Jr. (1995) *Protein Eng. 8*, 593−599.
11. Hayashi, A., Suzuki, T., and Shin, M. (1973) *Biochim. Biophys. Acta 310*, 309−316.
12. Scott, E. E., and Gibson, Q. H. (1997) *Biochemistry 36*, 11909−11917.
13. Monod, J., Wyman, J., and Changeux, J.-P. (1965) *J. Mol. Biol. 12*, 88−118.
14. Otwinowski, Z., and Wladek, M. (1997) *Methods Enzymol. 276*, 307−326.
15. Kissinger, C. R., Gehlhaar, D. K., and Fogel, D. B. (1999) *Acta Crystallogr. D55*, 484−491.
16. Brunger, A. T., Adams, P. D., Clore, G. M., DeLano, W. L., Gros, P., Grosse-Kunstleve, R. W., Jiang, J. S., Kuszewski, J., Nilges, M., Pannu, N. S., Read, R. J., Rice, L. M., Simonson, T., and Warren, G. L. (1998) *Acta Crystallogr. D54*, 905−921.
17. Jiang, J. S., and Brunger, A. T. (1994) *J. Mol. Biol. 243*, 100−115.
18. Read, R. J. (1986) *Acta Crystallogr. A42*, 140−149.
19. Kleywegt, G. J. (1996) *Acta Crystallogr. D52*, 842−857.
20. Collaborative Computational Project No. 4 (1994) *Acta Crystallogr. D50*, 760−763.
21. Berman, H. M., Westbrook, J., Feng, Z., Gilliland, G., Bhat, T. N., Weissig, H., Shindyalov, I. N., and Bourne, P. E. (2000) *Nucleic Acids Res. 28*, 235−242.
22. Scott, E. E., Gibson, Q. H., and Olson, J. S. (2001) *J. Biol. Chem. 276*, 5177−5188.
23. Zamparelli, C., Verzili, D., Boffi, A., Chiancone, E., Takahashi, S., Rousseau, D. L., Regan, R., and Gibson, Q. H. (1997) *Arch. Biochem. Biophys. 339*, 275−282.
24. Royer, W. E., Jr., Knapp, J. E., Strand, K., and Heaslet, H. A. (2001) *Trends Biochem. Sci. 26*, 297−304.
25. Heaslet, H. A., and Royer, W. E., Jr. (1999) *Structure 7*, 517−526.
26. Andersen, M. E., and Gibson, Q. H. (1971) *J. Biol. Chem. 246*, 4790−4799.
27. Heaslet, H. A., and Royer, W. E. (2001) *J. Biol. Chem. 276*, 26230−26236.
28. Mitchell, D. T., Kitto, G. B., and Hackert, M. L. (1995) *J. Mol. Biol. 251*, 421−431.
29. Ferrin, T. E., Huang, C. C., Jarvis, L. E., and Langridge, R. (1988) *J. Mol. Graphics 6*, 13−27.
30. Esnouf, R. M. (1997) *J. Mol. Graphics 15*, 132−134.
31. Merritt, E. A., and Bacon, D. J. (1997) *Methods Enzymol. 277*, 505−524.
32. Petruzzelli, R., Goffredo, B. M., Barra, D., Bossa, F., Boffi, A., Verzili, D., Ascoli, F., and Chiancone, E. (1985) *FEBS Lett. 184*, 328−332.
33. Mauri, F., Omnaas, J., Davidson, L., Whitfill, C., and Kitto, G. B. (1991) *Biochim. Biophys. Acta 1078*, 63−67.
34. Fushitani, K., Matsuura, M. S., and Riggs, A. F. (1988) *J. Biol. Chem. 263*, 6502−6517.
35. Xie, Q., Donahue, R. A., Jr., Schneider, K., Mirza, U. A., Haller, I., Chait, B. T., and Riggs, A. F. (1997) *Biochim. Biophys. Acta 1337*, 241−247.

BI011071T